ISIJ International, Vol. 44 (2004), No. 11, pp. 1826–1834

An Application of Bingham Model to Viscous Fluid Modeling of Solid Flow in Moving Bed

Hiroshi NOGAMI and Jun-ichiro YAGI

Institute of Multidisciplinary Research for Advanced Materials, Tohoku University, 2-1-1 Katahira, Aoba-ku, Sendai 980-8577 Japan.

(*Received on June 14, 2004; accepted in final form on August 9, 2004*)

Solid flow plays important roles in a moving bed reactor, for example, it determines the path and the residence time of the solid reactants as well as the stress distribution. The continuum models are useful for the kinetic based process analysis since their simplicity and computation load, although the discrete element approach is capable of estimating not only the particle motion but also the stress distribution in the bed. One of the continuum approaches is viscous fluid model. It is able to estimate solid flow pattern although it needs to appropriately determine the shape of stagnant region and viscosity before the simulation. In this study the Bingham model, which is the simplest shear rate-shear stress model of plastic fluid, is applied to the viscous fluid model of bulk solid flow within packed bed. This model successfully reproduce solid flow pattern in packed bed without setting stagnant zone, and the rheological properties can be obtained from simple preliminary experiments. Therefore, the viscous fluid model with the Bingham model is considered as a useful solid flow model for process analysis of moving bed reactors.

KEY WORDS: solid flow; simulation; viscous flow modeling; Bingham model; blast furnace.

1. Introduction

The motion of solid materials in moving bed reactors is one of the important factors in operation and design of the reactors because it determines the residence time of solid reactants, the feeding rate of materials to reaction area, formation of dead zone, the stress working on the reactor facilities, and so on. The particle bed shows the following characteristics. It generates fundamentally no tension to the tensile force while it does resistance force to compression force. It forms anisotropic stress field when the bed undergoes deformation. With these characteristics the granular bed in the moving bed reactor shows intermittent descent and formation of stagnant zone.

Various methods to estimate the flow behavior of granular materials in hoppers and bins have been proposed. The major purposes of these methods are on the evaluation of powder pressure working on the vessel or the control of discharging rate, thus they mainly focus on the stress distribution within the beds. Contrarily the flow patterns, namely the path and the residence time, of solid reactants given under the perfect material balance are required for the process analyses of moving bed reactors.

The mathematical models of the solid motion in the moving bed that can be applied to the process analysis are generally classified into three approaches. One of the approaches is to track numerous individual particles that compose the bed, and is called "Discrete Element Method (DEM)" or "Discrete Particle Method (DPM)".[1] In this method, the contact forces among particles or between a particle and the wall are described by the Voigt model that consists of springs, dash pods and sliders. The summation of these forces acting on a particle is included in the equation of motion of the particle of interest. This procedure is applied to all the particles considered, consequently the motion of the moving bed is given. This approach was applied to the charging of burden materials and the segregation behavior in the area of ironmaking.[2–4] Recently for the purposes of avoiding malfunction of blast furnaces or more detailed discussion on burden materials descent, this method has been applied to the analyses of particle motion in blast furnace cohesive zone,[5] raceway[6–8] and hearth[9,10] regions.

Second approach handles particle bed as an artificial continuum, and solves the relation between internal stress and deformation using the technique of materials mechanics. Katayama *et al.*[11] assumed elastoplasticity as stress–strain relation, and showed that the Drucker–Prager plasticity model, one of the isotropic elastoplastic model for concrete, soil or other geomaterials, was successfully reproduced the stress and the velocity distributions in a blast furnace. This method was applied to the stress analysis during packing and after ignition of blow-in operation of Kokura #2 BF,[12] and successfully reproduced actually measured variation of stress distribution in the furnace. Zaïmi *et al.*[13–15] used hypo-plasticity as stress–strain relationship and succeeded to calculate deadman shape and stress distribution in a small cold model of blast furnace.

Third approach treats the granular bed as an artificial fluid and describes the movement of the bed by the equation of motion of fluids. The simplest method assumes the plug flow, and gives the averaged velocity over the reactor cross section as the solid velocity. Although this method is

applicable only to one-dimensional analysis of the simple-shaped reactors, it has been applied to various reactor including blast furnace due to its simplicity.[16–18] Multi-dimensional process analysis usually requires flow analysis on corresponding dimension framework. The potential flow model and the kinematic model[19] are widely used in the multi-dimensional flow analysis of moving beds. The potential flow model describes the granular flow by the potential flow, which is a non-vortex flow, and the kinematic model assumes the horizontal velocity component of a particle is proportional to the horizontal gradient of the vertical velocity component. These models have been applied to the process analyses of moving bed reactors including blast furnace due to their simplicity.[20–22] The fundamental equations of these models are liner equations, thus they can be solved without heavy computational load in general. The authors[23] proposed a method to describe the flow of granules bed by using the Navier–Stokes equation, the equation of motion of viscous fluid. The solid flow in moving beds were successfully reproduced using appropriately selected viscosity.

Among three approaches, the DEM is considered the most accurate and widely applicable method because it is able to estimate the formation of stress field in the bed as well as the particle motion owing its feature, which tracks the trajectories of numerous particles with considering all forces acting on each particle. It, however, needs huge computational resources and time for the analysis of actual processes due to the number of particles to be pursued. Thus, a real-scale analysis of large scale moving bed process by this method is practically difficult at present. The approaches based on materials mechanics treat constitutive equations having different form with the equations of mass and heat balances. This makes the numerical implementation of the model more complicated and the coupling with the other phases difficult. The techniques based on the fluid dynamics deal with the continuity and the momentum equations that can be summarized in the same form with the heat and the material balance equations. Thus common numerical procedures for solving the equation can be introduced and reduce the computational complexity. In addition, this method can give the perfect material balance with its nature. This feature provides accurate estimation of fields of reaction and heat transfer.

The authors have been using the approach of the computational fluid dynamics as a solid flow model of an operation simulator of blast furnace,[24–26] and confirmed its validity from a number of operation simulations.[27,28] These computations, however, assumed the Newtonian fluid, and it was necessary to give the shape of stagnant zone in the bottom of the furnace. In addition, the method to determine the viscosity has yet to be established. In this study, an application of the Bingham model, one of the simplest shear stress–shear rate relation of the plastic fluids as rheological properties of viscous fluid modeling of solid flow in a moving bed to deal with these problems.

2. Model for Flow Analysis of the Bingham Fluid

The solid flow behavior is described by the continuity equation and equation of motion in the fluid dynamic modeling. Under the assumptions of steady state and axisymmetry, the solid flow is described by the two-dimensional motion on the plane that includes both symmetric and radial axes. In this two-dimensional plane, governing equations are described as follows.

Continuity equation:

$$\frac{\partial}{\partial x}(\rho u)+\frac{1}{r}\frac{\partial}{\partial r}(r\rho v) \quad \text{.....(1)}$$

Momentum balance equations:

$$\frac{\partial}{\partial x}(\rho uu)+\frac{1}{r}\frac{\partial}{\partial r}(r\rho vu) = -\frac{\partial p}{\partial x}+\frac{\partial}{\partial x}\left(2\eta_{\text{eff}}\frac{\partial u}{\partial x}\right)+\frac{1}{r}\frac{\partial}{\partial r}\left\{r\eta_{\text{eff}}\left(\frac{\partial v}{\partial x}+\frac{\partial u}{\partial r}\right)\right\} \quad \text{.....(2)}$$

$$\frac{\partial}{\partial x}(\rho uv)+\frac{1}{r}\frac{\partial}{\partial r}(r\rho vv) = -\frac{\partial p}{\partial r}+\frac{\partial}{\partial x}\left\{2\eta_{\text{eff}}\left(\frac{\partial v}{\partial x}+\frac{\partial u}{\partial r}\right)\right\} + \frac{1}{r}\frac{\partial}{\partial r}\left(2r\eta_{\text{eff}}\frac{\partial u}{\partial r}\right)-2\eta_{\text{eff}}\frac{v}{r^2} \quad \text{.....(3)}$$

The granular bed in the moving bed deforms in the region in which the shear stress exceeds a certain value. The plug flow region is clearly formed in a columnar bed. In this study the particle bed in a moving bed is treated as plastic fluid, and the Bingham model is applied as its shear stress–shear rate relationship. The Bingham fluid is rigid when the shear stress is smaller than the critical value (τ_0: yield stress), and starts to flow when the shear stress exceeds this value. In the flowing region the shear stress and shear rate show a linear relation. The relation between stress τ and sheer rate $\dot{\gamma}$ can be described as follows.

$$\left.\begin{array}{ll}\tau=\tau_0+\eta\dot{\gamma} & \text{for } \tau>\tau_0\\ \dot{\gamma}=0 & \text{for } \tau\leqq\tau_0\end{array}\right\} \quad \text{.....(4)}$$

in this equation, sheer rate is given by the following equation in two-dimensional axisymmetric coordinate system.

$$\dot{\gamma}=\sqrt{2\left\{\left(\frac{\partial u}{\partial x}\right)^2+\left(\frac{v}{r}\right)^2+\left(\frac{\partial v}{\partial r}\right)^2\right\}+\left(\frac{\partial v}{\partial x}+\frac{\partial u}{\partial r}\right)^2} \quad \text{.....(5)}$$

The effective viscosity of the Bingham fluid is determined by the shear stress and the sheer rate.

$$\eta_{\text{eff}}=\begin{cases}\eta+\dfrac{\tau_0}{\dot{\gamma}} & \text{for } \tau>\tau_0\\ \infty & \text{for } \tau\leqq\tau_0\end{cases} \quad \text{.....(6)}$$

The magnitude of shear stress equals to yield stress ($\tau=\tau_0$) when the sheer rate equals to zero ($\dot{\gamma}=0$). In the flow analysis, the flow field is determined by the momentum balance

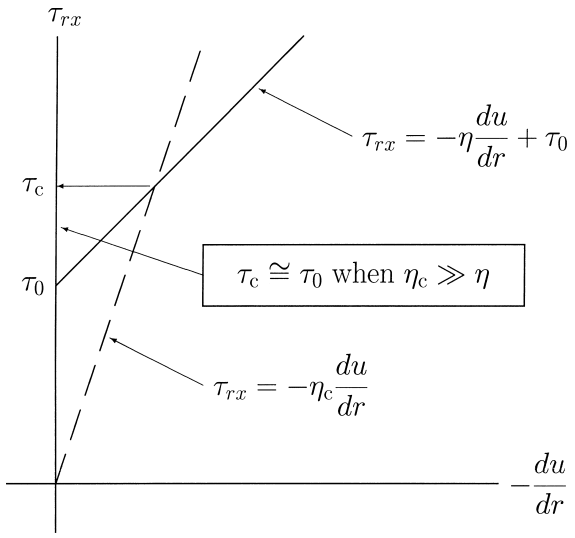

Fig. 1. Definition of virtual yield stress (τ_c).

including shear stress due to viscosity, consequently the flow field and stress field are closely coupled each other. In the determination of yielding of the Bingham fluid, however, rather the flow field determines the stress field than the stress field form the flow field. Thus the situation $\dot{\gamma}=0$ is hardly occur in the calculation of flow field. Additionally, infinite large viscosity is unable to be set in the actual numerical implementation. Therefore, following stress–sheer rate model shown in **Fig. 1** is introduced. The Bingham fluid is rigid until the shear stress generated in the fluid exceeds the yield stress. Thus the stress–shear rate relation moves upward on the ordinate from its origin in Fig. 1. Once the shear stress becomes larger than the yield stress, the fluid starts to flow, and the stress–shear rate relation follows the line of $\tau_{rx}=\tau_0-\eta(du/dr)$. In this study a finite but enough large viscosity η_c is applied for the rigid area. Thus the stress–shear rate relation varies with the line of $\tau_{rx}=-\eta_c(du/dr)$ with increase in shear stress. When the shear stress exceeds the value at the intersection point of this line and the line of $\tau_{rx}=\tau_0-\eta(du/dr)$, stress–shear rate relation moves along the latter line. The magnitude of the stress at this intersection point is defined as virtual yield stress, and its value is given by the following equation.

$$\tau_c=\eta_c\tau_0/(\eta_c-\eta) \quad \text{.....(7)}$$

The virtual yield stress takes the close value to the yield stress of the Bingham fluid when the η_c is enough large.

The equations of continuity and momentum balance, shown as Eqs. (1) through (3), were discretized using the control volume method, one of the finite difference techniques. The SIMPLER algorithm[29] was introduced to couple pressure field and material balance. The algebraic simultaneous equations that were derived through the discretizing of the above equations were solved using a line-by-line method with under relaxation iteration.

3. Flow Analysis of the Bingham Fluid

To validate the model for flow analysis of the Bingham fluid, the velocity distribution in a straight pipe was simulated. The analysis was performed for the situation that the

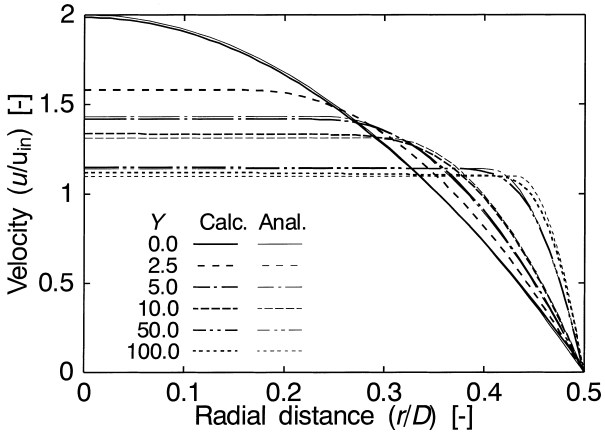

Fig. 2. Comparison of velocity distributions at outlet by numerical simulation and analytical solution.

Bingham fluid flowed into a pipe having diameter D of 0.02 m and length L of 0.1 m with uniform velocity distribution u_{in}. The density and the yield viscosity of the fluid and the Reynolds number ($Re=Du_{in}\rho/\eta$) were set at 1.0 kg/m^3, 3.8×10^{-2} Pa·s and 5.0, respectively. The yield stress was varied in six levels as a parameter for the simulation, namely 0, 90.3, 181, 361, 1 810 and 3610 Pa. Corresponding Yield numbers ($Y=\tau_0R/(\eta u_{in})$) for these yield stress respectively were 0, 2.5, 5, 10, 50 and 100.

With the assumption of axisymmetry, the flow pattern of the Bingham fluid was computed in one side of longitudinal cross section including the center axis of the pipe. This plane is divided into 200×50 equally spaced grids in axial and radial direction, respectively. Note that the viscosity of plug flow region takes the value two thousand times as yield viscosity.

Figure 2 compares the radial distribution of axial velocity component at the outlet of the pipe and the analytical distribution of well developed Bingham flow. The analytical solution of the velocity distribution of the Bingham fluid is given by the following equations taking the balance between shear stress within the fluid and pressure drop as driving force for the pipe flow.

$$u=\begin{cases}\dfrac{\Delta PR^2}{4\eta L}\left\{1-\left(\dfrac{r}{R}\right)^2\right\}-\dfrac{\tau_0 R}{\eta}\left(1-\dfrac{r}{R}\right) & \text{for } r>r_0\\ \dfrac{\Delta PR^2}{4\eta L}\left(1-\dfrac{r_0}{R}\right)^2 & \text{for } r\le r_0\end{cases} \quad \text{.....(8)}$$

the term r_0 in this equation is the radius of plug flow region and given as $r_0=2\tau_0L/\Delta P$. The overall pressure drop ΔP through the pipe is determined to provide the given volumetric flow rate of the Bingham fluid:

$$Q=\frac{\pi\Delta PR^4}{8\eta L}\left\{1-\frac{4}{3}\left(\frac{\tau_0}{\tau_R}\right)+\frac{1}{3}\left(\frac{\tau_0}{\tau_R}\right)^4\right\}$$

$$\text{where } \tau_R=\Delta PR/2L \quad \text{.....(9)}$$

The velocity distribution was obtained with this pressure drop. In this equation, the term τ_R is the shear stress at the wall, and expressed as follows.

$$\tau_R = \frac{\Delta P R^4}{8\eta L} \quad \text{.....(10)}$$

For the case of $Y=0$, the yield stress of the fluid is zero, in other words the fluid becomes the Newtonian fluid, thus the velocity distribution at the outlet shows the parabolic distribution. For the other Yield numbers, the plug flow region is formed around the center axis, and its diameter increases with increase in the Yield number. The numerical results reproduced the diameter and velocity of the plug flow region of analytical ones at any Yield numbers. Therefore, it is considered that the simulation method of the Bingham flow proposed in this study is valid.

4. Rheological Properties of Moving Granular Bed

The motion of particles in a moving bed is generally slow, and it is mainly governed by the mechanical force balance including friction and powder pressure within the bed, not by the inertia of the particle. Thus the rheological characteristics is important issues in the viscous fluid modeling of the granular bed motion. The authors determined the viscosity by the parameter fitting through various preliminary simulations in the previous viscous fluid modeling by the Newtonian fluid.[23] In the Bingham modeling of the solid flow, two parameters, namely the yield viscosity and the yield stress, have to be set in prior to the computation. Therefore the procedure of the parameter fitting becomes complicated, and it does not always give only a combination of the parameters. In addition, these parameters vary depending on the operating condition, like facility, particles, discharging rate, and so on. Consequently the parameter fitting based on the comparison between computational and experimental results has to be carried out for accurate simulation in each case. Thus it is considered that the determination of the particle bed properties as continuous fluid without fitting process expands the applicability of the viscous fluid modeling of the solid flow. The rheological properties of the granular bed was discussed based on the velocity distribution in columnar moving bed.

4.1. Method of Data Processing

Takahashi and co-workers[30–33] measured the flow patterns of the granular beds in vertical columns. Their work provides the particle diameter, angle of repose, internal friction angle, wall friction angle, bulk density (particle density and voidage), column diameter, average velocity of the bed (particle flow rate) and the diameter of plug flow region. The diameter of the plug flow region in well developed Bingham flow is analytically given when the four parameters are known, namely, the flow rate, the fluid density, the yield stress and yield viscosity. The bulk density and discharging rate of the particle bed correspond respectively to the fluid density and the flow rate. The diameter of the plug flow region is supplied as the result of their measurements. Therefore, given one of the yield stress or the yield viscosity, the other one can be obtained. In this section, the yield stress of the packed bed is estimated by the following procedure, and the yield viscosity is treated as the unknown parameter. The yield stress of the bed was determined based on the Janssen's equation although the state of stress field in fixed and moving beds are different each other. First the vertical powder pressure is calculated by the Janssen's equation.

$$P_v = \frac{\rho D}{4\mu_w K}\left\{1-\exp\left(-\frac{4\mu_w K}{D}\right)h\right\} \quad \text{.....(11)}$$

This is converted to the horizontal powder pressure ($P_h=P_v((1-\sin\phi_i))/(1-\sin\phi_i)$). Finally the yield stress is obtained by multiplying the internal friction coefficient ($\tan\phi_i$) to the horizontal powder pressure. The yield viscosity of the bed is calculated by Eq. (6) substituting this yield stress and the diameter of the plug flow region. Note that the yield stress of the bed was calculated at the bed depth of three times as the bed diameter because Takahashi *et al*. stated that the velocity distribution showed no variation when the depth is larger than three times as bed diameter.

4.2. Results

The velocity distributions obtained for the moving bed of glass bead, sand, silica sphere, alumina ball, soy bean, millet, coal and salt. The results are summarized in **Table 1**. The ranges of the Yield number are from 20 to 50 for the glass bead and from 400 to 1 200 for the small sand. The large sand, the silica spheres, the alumina balls and soy bean show the similar Yield number as glass beads while the coal and the salt are in the similar range as small sand. Namely, the particles having smooth surface and spherical shape have the Yield number from 20 to 50, and this parameter of the irregular particles have the range from 400 to 1 200.

The relation ship between the Yield number and the ratio of duct diameter to particle diameter, the Yield number and the internal friction angle, and the yield viscosity and the internal friction angle are shown in **Figs. 3** through **5**. The Yield number tends to increase with the increases in the diameter ratio and the internal friction angle. The yield viscosity shows the tendency to decrease with increase in the internal friction angle. The plug flow region of the Bingham flow tends to expand when the ratio of the yield stress to the yield viscosity increases, namely, either the increase in yield stress or the decrease in yield viscosity. For the solid flow in the vertical columns, the plug flow region expands with the increase in the column diameter even the particle diameter is constant. Thus the Yield number of the granular bed increases with the diameter ratio of the column to the particle. The plug flow region is enlarged when the internal friction angle of the bed increases, and the Yield number increase with the internal friction angle.

5. Solid Flow Simulation in a Moving Bed

5.1. Method of Solid Flow Analysis

The equations of motion for the Bingham fluid were used as the governing equation for the solid flow simulation. For the ordinary analysis of the Bingham flow, the fluid properties, like density, yield stress, yield viscosity, and so on, are constant. Contrarily the rheological properties of the moving bed, the yield stress and the yield viscosity, was assumed depending on the powder pressure. The vertical distribution of vertical powder pressure in the bed was calcu-

Table 1. Properties of bulk solid particles.

Material	d_p [mm]	ϕ_i [deg]	ϕ_w [deg]	ρ_b [kg/m^3]	u_{ave} [m/s]	D [m]	r_{core}/R [-]	τ_0 [Pa]	η [Pa·s]	Y [-]	Re [-]
G.B.	1	35	9	1550	3.59e-4	0.1	0.81	675	1840	51.0	3.02e-5
G.B.	1	35	9	1550	8.02e-4	0.1	0.8	675	920	45.8	1.35e-4
G.B.	1	35	9	1540	9.84e-4	0.1	0.81	675	673	51.0	2.25e-4
G.B.	1	35	9	1540	2.28e-3	0.1	0.79	671	357	41.3	9.84e-4
G.B.	1	35	9	1550	6.31e-3	0.1	0.79	676	130	41.3	7.54e-3
G.B.	1	35	9	1550	2.67e-3	0.1	0.79	676	307	41.3	1.35e-3
G.B.	1	35	9	1525	1.54e-3	0.1	0.79	665	523	41.3	4.49e-4
G.B.	1	35	12	1590	6.10e-4	0.0529	0.79	339	356	41.3	1.44e-4
G.B.	1	35	12	1590	2.27e-3	0.0529	0.79	339	95.6	41.3	2.00e-3
G.B.	1.5	35	9	1600	7.12e-3	0.1	0.7	698	257	19.3	4.44e-3
G.B.	1.5	35	9	1525	7.47e-3	0.1	0.7	665	233	19.1	4.89e-3
G.B.	4	35	8	1513	1.12e-3	0.1	0.73	677	1260	24.1	1.35e-4
G.B.	4	35	8	1538	2.41e-3	0.1	0.72	689	643	22.2	5.76e-4
Sand	0.2	48	28	1430	7.43e-3	0.1	0.89	446	18.9	158	0.0561
Sand	0.2	48	28	1380	7.30e-5	0.1	0.96	430	239	1230	4.21e-5
Sand	0.2	48	28	1370	3.60e-4	0.1	0.95	427	75.4	787	6.54e-4
Sand	0.2	48	28	1390	7.97e-4	0.1	0.95	434	34.5	787	3.21e-3
Sand	0.2	48	28	1400	2.36e-3	0.1	0.95	437	11.7	787	0.0281
Sand	0.2	48	28	1430	4.20e-3	0.1	0.94	434	6.55	787	0.0916
Sand	0.2	42	28	1430	2.32e-3	0.0529	0.93	225	6.45	398	0.0272
Sand	0.2	42	28	1430	0.0114	0.0529	0.93	225	1.31	398	0.657
Sand	0.34	48	28	1478	3.93e-3	0.1	0.94	464	10.9	542	0.0534
Sand	0.34	48	28	1380	7.57e-5	0.1	0.96	430	230	1230	4.53e-5
Sand	0.34	48	28	1370	3.65e-4	0.1	0.95	427	74.3	787	6.73e-4
Sand	0.34	48	28	1390	7.97e-4	0.1	0.95	434	34.5	787	3.21e-3
Sand	0.34	48	28	1400	2.36e-3	0.1	0.95	437	11.8	786	0.0281
Sand	0.34	48	28	1430	4.14e-3	0.1	0.94	446	9.92	543	0.0597
Sand	0.34	48	28	1430	2.32e-3	0.0529	0.93	236	6.75	398	0.0260
Sand	0.34	48	28	1430	0.0114	0.0529	0.93	236	1.37	398	0.627
Sand	2.2	48	28	1660	1.97e-3	0.1	0.84	518	180	73.1	1.83e-3
Sand	2.2	48	28	1680	5.49e-3	0.1	0.83	524	83.4	57.2	0.0111
Sand	2.2	48	28	1690	8.59e-3	0.1	0.81	527	60.1	51.0	0.0242
Sand	2.2	48	28	1700	4.84e-3	0.0529	0.74	280	58.7	26.1	7.42e-3
Sand	2.2	48	28	1700	0.0111	0.0529	0.74	280	25.6	26.1	0.0390
Silica	4	40	10	889	3.29e-3	0.1	0.7	382	304	19.1	9.61e-4
Silica	4	40	10	889	6.06e-3	0.1	0.68	382	191	16.5	2.82e-3
Alumina	4.4	30	11	932	7.24e-3	0.1	0.7	367	133	19.1	5.09e-3
Alumina	4.4	30	11	939	3.15e-3	0.1	0.65	369	435	13.5	6.80e-4
Alumina	4.4	30	11	880	5.35e-4	0.1	0.72	346	1460	22.2	3.23e-5
Soybean	6.4	35	20	750	0.0121	0.1	0.67	245	65.8	15.4	0.0138
Millet	1.3	55	33	783	4.23e-4	0.1	0.99	227	1.34	20000	0.0247
Millet	1.3	55	33	786	2.71e-3	0.1	0.99	228	0.210	20000	1.01
Millet	1.3	55	33	785	0.0107	0.1	0.99	228	0.0532	20000	15.8
Millet	1.3	55	33	822	3.65e-3	0.0529	0.87	126	8.15	112	0.0195
Coal	4.1	60	40	740	6.88e-3	0.1	0.96	193	1.14	1230	0.448
Coal	4.1	60	40	740	0.0287	0.1	0.96	193	0.272	1230	7.80
Salt	0.5	50	30	1250	1.02e-3	0.0529	0.89	201	32.9	158	2.05e-3
Salt	0.5	50	30	1260	2.01e-3	0.0529	0.89	202	16.8	158	7.96e-3

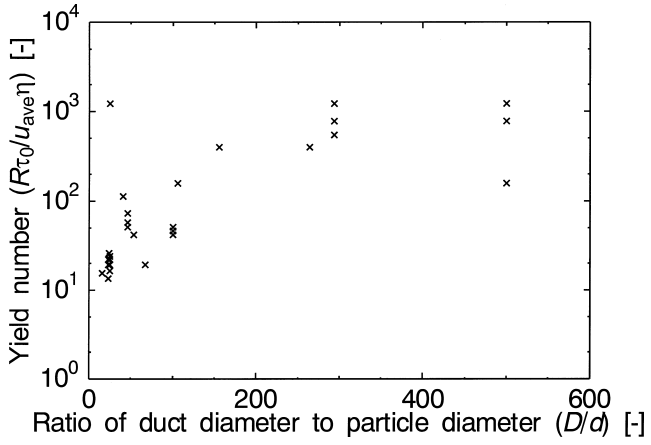

Fig. 3. Relation between ratio of duct diameter to particle diameter and Yield number.

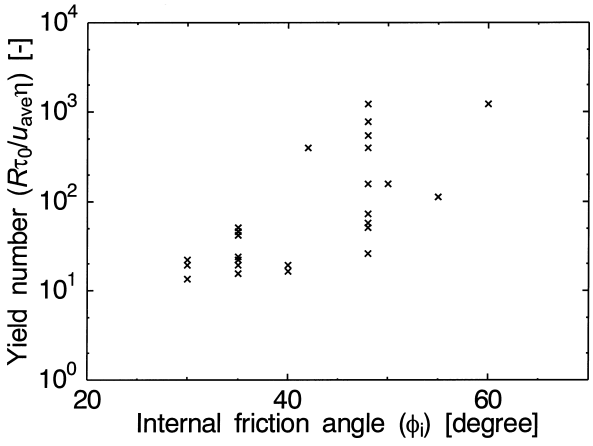

Fig. 4. Relation between internal friction angle and Yield number.

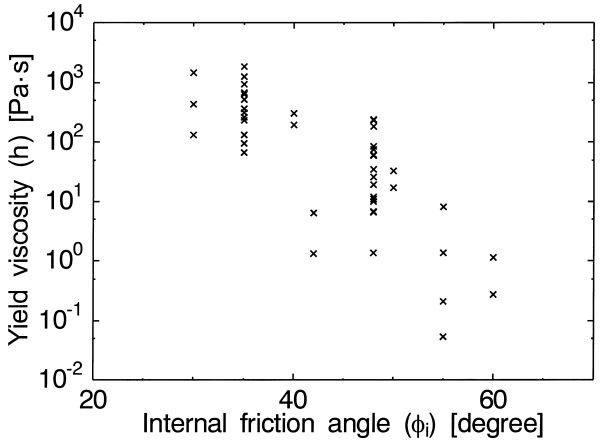

Fig. 5. Relation between internal friction angle and yield viscosity.

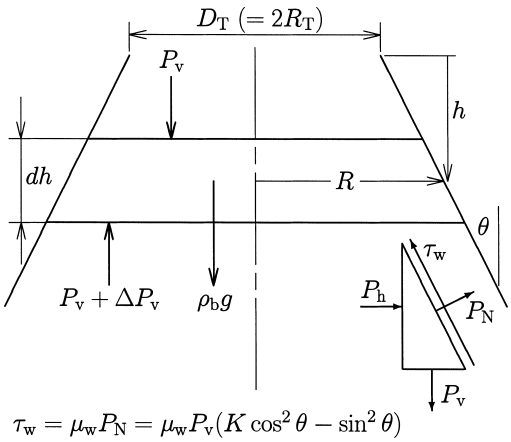

Fig. 6. Powder pressure in tapered bed.

lated by the Janssen's equation. For the tapered column like blast furnace shown in **Fig. 6**, the powder pressure distribution was estimated by integrating the following equation.

$$\frac{dP_h}{dh} = \rho_b g - 2\mu_w(K\cos^2\theta - \sin^2\theta)\frac{P_v}{R_0 + h\tan\theta} \quad \text{.....(12)}$$

With this obtained vertical pressure at each level was converted to the horizontal powder pressure. The integration of the governing equation of the Bingham flow was performed through the iterating calculation. The streamlines of the granular bed were computed in each calculation step. The shearing deformation was assumed to arise along a streamline, and the yield stress and yield viscosity were determined based on this direction. The yield stress was given by multiplying the internal friction coefficient to the powder pressure in the perpendicular direction to the streamline. Although the vertical stress generated within the packed bed is usually given by the oval of vertical pressure, it is calculated by the linear interpolation between vertical and horizontal powder pressure for the computational simplicity. The yield viscosity was calculated using this yield stress and the Yield number, which was set prior to the computation.

5.2. Results

The computations were performed for a small cold model of blast furnace shown in **Fig. 7**. The physical model has the packing height of 332 mm and the bottom diameter of 196 mm. The side wall higher than 112 mm is tapered and the diameter decreases with height to 130 mm at the top. A circular disk plate having the diameter of 168 mm is settled horizontally at the bottom of the cold model, and the packed particles are discharged from the annular slit formed between model wall and the disk plate. The properties and discharging condition of the packed particles are summarized in **Table 2**. The Reynolds number and the Yield number used in the simulation were set at 3.8×10^{-3} and 100, respectively.

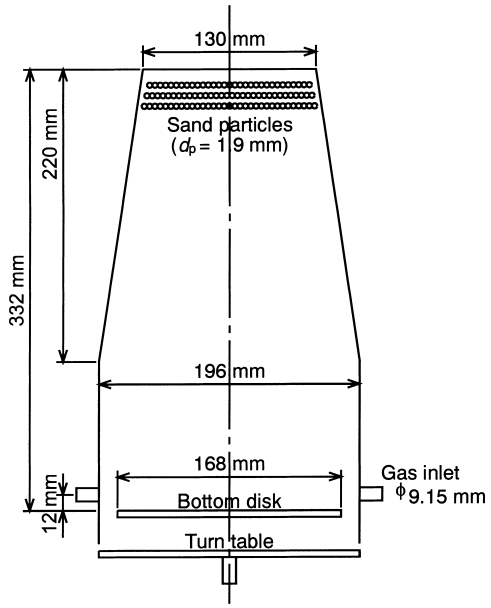

Fig. 7. Schematic diagram of experimental apparatus.

Table 2. Properties of sand particles and flow conditions.

d_p	0.0019	m
ρ_p	2600.0	kg/m^3
θ_i	45	deg.
θ_w	25	deg.
ε	0.51	
W	5.97×10^{-3}	kg/s
Re	3.8×10^{-3}	
Y	100	

The comparison of the calculated time lines among the Newtonian flow, the Bingham flow with uniform properties and the Bingham flow with powder-pressure dependent properties is shown in **Fig. 8**. The measured time lines run almost horizontally in the upper part of the cold model. The effect of wall friction becomes remarkable and the delay of descent appears near the wall when the particles reach the lower part of the rig of which side wall is vertical. In the bottom part of the apparatus, the stagnant zone is formed on the bottom plate and the formation of the funnel flow is observed between this stagnant zone and the cold model wall.

In the calculation assuming the Newtonian fluid, the shape of the stagnant zone on the bottom plate was specified following the method of Chen *et al.*,[23,34] and the viscosity of 0.07 Pa·s was used. The solid flow simulation with the Newtonian fluid well reproduced the measured result although the descending velocity slightly slowed due to the

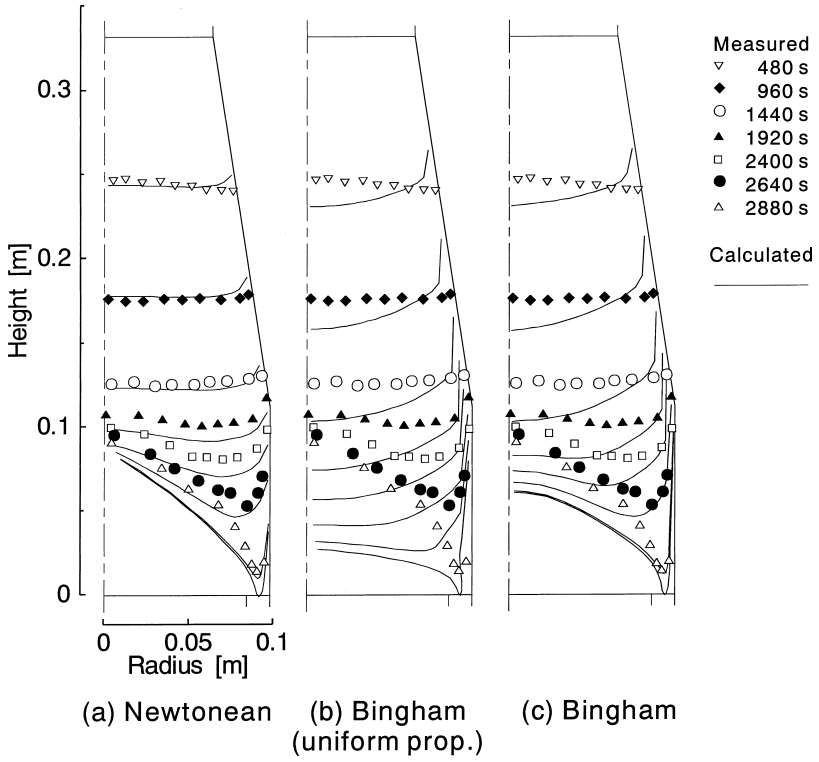

Fig. 8. Comparison of time lines calculated by three models.

diameter expansion in the upper part. The Bingham flow with uniform properties showed the large descending delay near the wall and formed the time lines inclining to the central part. For this case the height of stagnant zone is underestimated, and the funnel flow region is formed only adjacent to the bottom. Contrarily the Bingham flow analysis taking into account the dependency of the properties on powder pressure distribution estimates higher deadman and well describes the formation of the funnel flow region due to the frictions of vertical wall and stagnant zone.

Both of the flow patterns of Bingham fluid shown in Fig. 8 showed fairly large dealy of descent near the upper wall and the inclined time lines to the central part, and these trends disagree with the experimental results. The reason for this tendency is considered that the above Bingham flow analyses used no slip boundary condition for the momentum balance equations on the wall boundary while the Newtonian analysis used the slip condition with wall friction evaluated by the Fanning's equation. This no slip condition was used expecting the formation of yield region near the wall. The particles near the inclined wall, however, show little velocity decrease while the effect of the wall friction is significant in the vicinity of the vertical wall. The powder pressure acting on the tapered wall expanding downward is considered smaller than one acting on vertical wall and almost uniform velocity distribution is formed in the upper part of the bed. Thus the slip condition was applied to the inclined wall while no slip condition was still used for the vertical wall as boundary conditions. **Figure 9** shows the time lines obtained using this treatment. With the slip condition for the inclined wall, the velocity decrease near the inclined wall becomes much smaller and the descending velocity in the central region slows compared with the results with the no slip condition. This tendency makes the time lines in the upper part more horizontally and closer

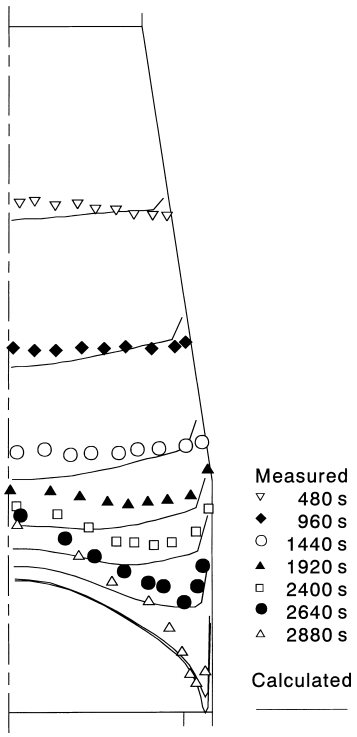

Fig. 9. Calculated timelines by using slip condition at shaft wall.

to the experimental result. The height of the stagnant zone on the bottom becomes higher with this variation of flow pattern in the upper part. The calculated time lines becomes closer generally to the measured ones. Even in this case the area of the deadman zone is still slightly underestimated, and the computed and measured time lines show a little discrepancy in the middle part in which the funnel flow starts to develop.

Recent solid flow simulation based on the elasto-

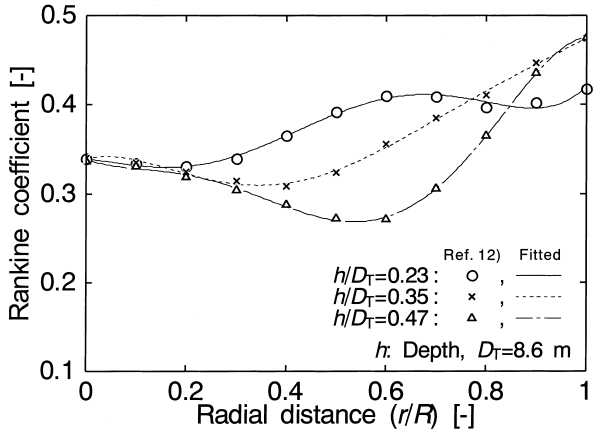

Fig. 10. Radial distributions of Rankine coefficient at different depths of taper shaped packed bed.

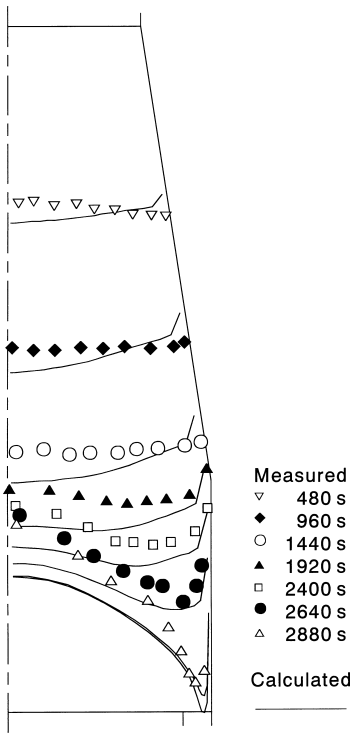

Fig. 11. Time lines calculated by using distributed Rankine coefficient.

plasticity[35] showed the stress field within the moving beds as well as the solid flow pattern. These results showed that the Rankine coefficient varied with radial position as well as with the depth in the bed with the tapered bed expanding downward. The variation of the Rankine coefficient shown in **Fig. 10**, which was obtained for the bed having top diameter of 8.6 m and wall inclination angle of 89 degree, was applied to the simulation. The Rankine coefficient is computed interpolating the distributions shown in Fig. 10 down to the depth $h/D_T=0.47$, and the radial distribution at $h/D_T=0.47$ was applied for the region lower than this depth. The calculated time lines using this distribution of the Rankine coefficient is shown in **Fig. 11**. With this treatment, the height of the deadman becomes slightly higher and the funnel flow is enhanced a bit, and the flow pattern comes closer to the measured one. The overall solid flow pattern, however, shows little variation, and still includes slight discrepancy with the measured solid movement. The Bingham model, the simplest shear rate-shear stress relationship of plastic fluid is considered unable to reproduce precisely the complex stress field formed in the lower part of the cold model of blast furnace. Therefore, for more accurate analysis of solid flow in moving beds based on the plastic fluid modeling, it is necessary to introduce more comprehensive or complicated description of rheological properties of the granular bed. The solid flow simulation based on the viscous fluid model with the Bingham model, nevertheless, is considered useful enough as the solid flow sub-model for the simulation of moving-bed reaction processes, because;

(1) The rheological properties used in the analysis can be determined through the simple preliminary experiment on velocity distribution using the vertical columnar moving bed.

(2) It is unnecessary to determine the shape of stagnant zone beforehand. The estimation of the stagnant zone shape formed in the center bottom of the bed with annular discharging is still an important issue. For example, although an empirical method to estimate the stagnant zone is proposed,[34] the effect of operation conditions are difficult to be reflected in this method. In addition, even the DEM approach which is considered most precise simulation method for granular bed movement needs more discussion for this issue.[9]

(3) Overall solid flow pattern with perfect material balance can be reproduced through simple boundary condition setting.

6. Conclusions

In this study the viscous fluid modeling of the particle bed flow is improved by applying the Bingham model as the shear stress–shear rate relationship. This treatment eliminate the necessity to determine the deadman shape before the computation, which was needed in the Newtonian fluid modeling. The yield stress and the yield viscosity that are only the rheological parameters of the Bingham fluid can be determined through the simple preliminary experiments. The discussion on the boundary condition at the wall for the momentum balance equations revealed that the application of the non-slip and slip conditions respectively for the vertical and overhanging inclined walls reproduce satisfactory the solid flow pattern in a cold model of blast furnace. Therefore the viscous fluid modeling with the Bingham model is considered useful as a solid flow model of the process analysis of the moving bed reactors.

Nomenclature

D	: Diameter	[m]
g	: Gravity	[m/s^2]
h	: Depth	[m]
L	: Length of pipe	[m]
P_h, P_v	: Horizontal and vertical powder pressure	[Pa]
ΔP	: Pressure drop in pipe	[Pa]
p	: Pressure	[Pa]
Q	: Volumetric flow rate	
R	: Radius of pipe	[m]
Re	: Reynolds number ($=Du_{in}\rho/\eta$)	[−]
r_0	: Radius of plug flow region ($=2\tau_0 L/\Delta P$)	[m]

r, x	: Radial and axial coordinate	[m]
u, v	: Radial and axial velocity component	[m/s]
u_{in}	: Average velocity	[m/s]
Y	: Yield number ($=\tau_0 R/(\eta u_{in})$)	[−]

Greek symbol

$\dot{\gamma}$	: Sheer rate	[s^{-1}]
η	: Yield viscosity	[Pa·s]
η_c	: Virtual viscosity	[Pa·s]
η_{eff}	: Effective viscosity	[Pa·s]
θ	: Wall inclination angle	[rad]
μ_w	: Wall friction coefficient	[−]
ρ	: Density	[kg/m^3]
ρ_b	: Density of bed	[kg/m^3]
τ	: Sheer stress	
τ_0	: Yield stress	[Pa]
τ_c	: Critical stress	[Pa]
τ_R	: Sheer stress at wall	[Pa]
ϕ_i	: Internal friction angle	[rad]

REFERENCES

1) P. A. Cundall and O. D. L. Strack: *Geotechnique*, **29** (1979), 47.
2) T. Tanaka, Y. Kajiwara and T. Inada: *Tetsu-to-Hagané*, **74** (1988), 2262.
3) Y. Kajiwara, T. Inada and T. Tanaka: *Tetsu-to-Hagané*, **75** (1989), 235.
4) S. Matsuzaki and Y. Taguchi: *CAMP-ISIJ*, **12** (1999), 127.
5) A. B. Yu, Z. Y. Zhou, S. J. Zhang, B. Wright and P. Zulli: Proc. of Int. Workshop on Sci. Tech. Innovative Ironmaking for aiming at Energy Half Consumption, ISIJ, Tokyo, (2003), 241.
6) K. Nakano and H. Yamaoka: *CAMP-ISIJ*, **14** (2001), 198.
7) K. Nakano and H. Yamaoka: *CAMP-ISIJ*, **16** (2003), 144.
8) H. Nogami and H. Yamaoka: Proc. of Int. Workshop on Sci. Tech. Innovative Ironmaking for aiming at Energy Half Consumption, ISIJ, Tokyo, (2003), 225.
9) H. Kawai and H. Takahashi: *ISIJ Int*., **44** (2004), 1140.
10) T. Nouchi, K. Takeda and A. Yu: *CAMP-ISIJ*, **16** (2003), 145.
11) K. Katayama, S. Wakabayashi, T. Inada, K. Takatani and H. Yamaoka: *Tetsu-to-Hagané*, **83** (1997), 91.
12) T. Inada, Y. Matsukura, M. Yaeda, S. Matsumura, S. Komatsu, T. Yamamoto and M. Onishi: *ISIJ Int*., **43** (2003), 1376.
13) S. A. Zaïmi, J.-B. Guillot, C. Petit and J. M. Steiler: ICSTI/ Ironmaking Conf. Proc., ISS, AIME, Warrendale, PA, (1998), 343.
14) S. A. Zaïmi, T. Akiyama, J.-B. Guillot and J. Yagi: *ISIJ Int*., **40** (2000), 322.
15) S. A. Zaïmi, T. Akiyama, J.-B. Guillot and J. Yagi: *ISIJ Int*., **40** (2000), 332.
16) Y. S. Cho and B. Joseph: *Ind. Eng. Chem. Process. Des. Dev*., **20** (1981), 314.
17) M. Kim and B. Joseph: *Ind. Eng. Chem. Process. Des. Dev*., **22** (1983), 212.
18) J. Adánez and F. G. Labiano: *Ind. Eng. Chem. Res.*, **29** (1990), 2079.
19) R. M. Nedderman and U. Tüzün: *Powder Technol*., **20** (1978), 24.
20) T. Sugiyama and M. Sugata: *Seitetsu Kenkyu*, **325** (1987), 34.
21) H. Yamaoka, Y. Kamei: *Tetsu-to-Hagané*, **73** (1988), 2254.
22) J. Wang, R. Takahashi and J. Yagi: *Kagaku Kougaku Ronbunshu*, **17** (1991), 179.
23) J. Chen, T. Akiyama, H. Nogami, J. Yagi and H. Takahashi: *ISIJ Int*., **33** (1993), 664.
24) P. R. Austin, H. Nogami, J. Yagi: *ISIJ Int*., **37** (1997), 458.
25) P. R. Austin, H. Nogami, J. Yagi: *ISIJ Int*., **37** (1997), 748.
26) J. A. Castro, H. Nogami and J. Yagi: *ISIJ Int*., **42** (2002), 44.
27) P. R. Austin, H. Nogami and J. Yagi: *ISIJ Int*., **38** (1998), 246.
28) J. A. Castro, H. Nogami and J. Yagi: *ISIJ Int*., **40** (2000), 637.
29) S. V. Patankar: Numerical Heat Transfer and Fluid Flow, Hemisphere Sci. Pub., Washington, USA, (1980), 133.
30) H. Takahashi and H. Yanai: *Kagaku Kogaku*, **35** (1971), 357.
31) H. Takahashi and H. Yanai: *Kagaku Kogaku*, **35** (1971), 1372.
32) H. Takahashi and H. Yanai: *Kagaku Kogaku*, **37** (1973), 1031.
33) H. Takahashi and Y. Honda: *Kagaku Kogaku Ronbunshu*, **18** (1992), 849.
34) H. Takahashi, K. Kushima and T. Takeuchi: *ISIJ Int*., **29** (1989), 117.
35) Sumitomo Metals: Private Communication, (1996).